energies

MDPI

Review

A Review on the Materials Science and Device Physics of Semitransparent Organic Photovoltaics

Nora Schopp [1] and Viktor V. Brus [2,*]

[1] Center for Polymers and Organic Solids, Department of Chemistry and Biochemistry, University of California Santa Barbara (UCSB), Santa Barbara, CA 93106, USA; nschopp@ucsb.edu
[2] Department of Physics, School of Sciences and Humanities, Nazarbayev University, Nur-Sultan City 010000, Kazakhstan
* Correspondence: viktor.brus@nu.edu.kz

Abstract: In this review, the current state of materials science and the device physics of semitransparent organic solar cells is summarized. Relevant synthetic strategies to narrow the band gap of organic semiconducting molecules are outlined, and recent developments in the polymer donor and near-infrared absorbing acceptor materials are discussed. Next, an overview of transparent electrodes is given, including oxides, multi-stacks, thin metal, and solution processed electrodes, as well as considerations that are unique to ST-OPVs. The remainder of this review focuses on the device engineering of ST-OPVs. The figures of merit and the theoretical limitations of ST-OPVs are covered, as well as strategies to improve the light utilization efficiency. Lastly, the importance of creating an in-depth understanding of the device physics of ST-OPVs is emphasized and the existing works that answer fundamental questions about the inherent changes in the optoelectronic processes in transparent devices are presented in a condensed way. This last part outlines the changes that are unique for devices with increased transparency and the resulting implications, serving as a point of reference for the systematic development of next-generation ST-OPVs.

Keywords: organic photovoltaics; semitransparency; organic semiconductors; device engineering; device physics

Citation: Schopp, N.; Brus, V.V. A Review on the Materials Science and Device Physics of Semitransparent Organic Photovoltaics. *Energies* **2022**, *15*, 4639. https://doi.org/10.3390/en15134639

Academic Editor: Jürgen Heinz Werner

Received: 23 May 2022
Accepted: 20 June 2022
Published: 24 June 2022

1. Introduction

Organic photovoltaics have emerged as a technology that reshapes the energy landscape. Their versatility and flexibility in design has moved them to the forefront of integrated energy harvesting solutions [1–3]. Besides offering mechanical flexibility and being lightweight, their solution-processability allows for low cost and high-throughput deposition methods [4–9]. However, the property that sets them most clearly apart is their optical tunability [10–13]. Bulk-heterojunction solar cells (BHJ) comprise a photoactive layer donor–acceptor blend based on polymeric and molecular components that can be chemically finetuned to absorb in the desired spectral region. With efficient photon-harvesting outside of the visible region of the spectrum, (semi-)transparent absorbers can generate electricity from the ultraviolet or infrared part of the spectrum. In combination with transparent electrode materials, they can be integrated into windows for net-zero-energy buildings and greenhouses or into windows of vehicles or displays [1,14–18].

To date, the predicted performance limitations of ST-OPVs exceed the currently reported efficiencies by far, in contrast to opaque OPVs, which underwent great PCE boosts in the past few years, now reaching PCEs of over 18% thanks to new material design, optimized processing and advanced interfacial engineering [19–23].

In this review, we will cover the material design principles for donors and acceptors for ST-OPVs, with focus on near IR-absorbing molecules, discuss transparent electrode materials and focus on the existing understanding of photoelectronic processes in ST-OPVs and the aspects that set them apart from their opaque counterparts.

2. Materials

2.1. Narrow Band Gap Polymer Donors

Although a manifold of highly efficient polymer donors exists in the field of OPVs, only a selection of them satisfies the optical requirements for semi-transparent OPVs. The most prominent strategy to achieve transparency is the band gap-narrowing of the p-type semiconducting polymers to achieve absorption in the near-IR. The conjugated chain of delocalized electrons in OPV polymer donors features a series of overlapping p_z orbitals with sp^2 or sp hybridization. When considering a conjugated system, the most intuitive way to narrow the band gap is the extension of the conjugation lengths that leads to the formation of continuous bands (Figure 1) [24–26]. For example, Liu et al.'s work on medium-sized chromophores demonstrates bandgap narrowing of the extended chromophores compared to their small molecule counterparts while maintaining good molecular orientation in the films, similar to that of polymeric materials [27]. Synthetic strategies that aim for high planarity and reduced rotational disorder are based on the concept of extending the conjugation lengths [28]. However, this approach reaches its limits quickly for extended polymer chains and little or no effect on the band gap may be observed as the effective conjugation lengths remain unchanged for such extended chains [29]. Therefore, other approaches are required.

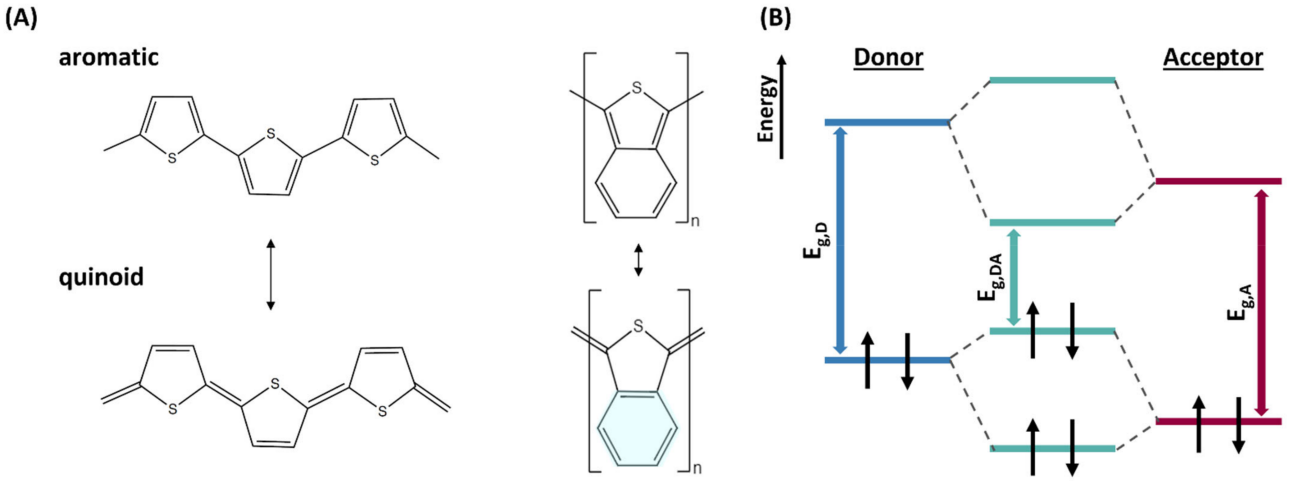

Figure 1. (**A**) Examples of aromatic and quinoid forms of polythiophene and polyisothiophene (left) and poly(isothianaphthene), stabilized by the benzene ring resonance energy upon formation of the quinoidal form. (**B**) Energy diagram of donor and acceptor moieties and hybrid orbitals of D-A type molecule/polymer.

The conjugated system can be represented by two resonance structures, the aromatic and the quinoidal form [7,28,30–32]. One of the main synthetic strategies to narrow the band gap of donor polymers is to stabilize the quinoidal form, such as by fusing a second ring to the polymer backbone that provides aromatic resonance stabilization energy upon formation of the quinoid form, as shown in Figure 1A. For example, the aromatic polymer polythiophene transforms to quinoidal poly(isothiophene), which is stabilized by a Benzene ring [28,32,33]. Although the aromatic form of this polymer has a band gap of $E_g \sim 2$ eV, band gaps as low as 0.5–1 eV have been reported for mixed aromatic-quinoidal polymer [33–35]. The fraction of the quinoidal form in such mixed polymers is directly correlated with the bond length alternation (BLA), which is defined as the average of the difference in length between the adjacent carbon–carbon bonds in a polyene chain and directly correlated with the band gap. With increasing quinoid contribution, the carbon−carbon single bonds between two adjacent rings adopt more double bond character and both the BLA and the band gap decrease [28–30]. For example, Takimiya et al., synthesized PBDTD4T with a band gap of 0.8 eV, and Salleo and Andersson et al. showed polymers based

on thiadiazoloquinoxaline with a bandgaps <0.7 eV [36,37]. A recent in-depth overview of quinoid polymers for OPVs can be found elsewhere [38].

Another prominent design strategy that dominates synthetic efforts are donor–acceptor (DA) type polymers, consisting of alternating electron-rich and electron-poor motives [31,32,39–43]. The interaction of the donor's highest occupied molecular orbital (HOMO) with the acceptors' HOMO leads to the formation of two hybrid orbitals of non-degenerate energy, thus one level being energetically lower than the HOMOs of the isolated moieties, as described by MO theory [44,45]. The same applies to the hybridization of the LUMOs of D and A, resulting in band gap narrowing, as schematically shown in Figure 1B. In addition, the alternation of electron-donating and withdrawing D and A units facilitates the formation of the quinoidal structure via the push–pulling effect and decreases the BLA, therefore, overlapping with the first mentioned design concept. Lastly, intermolecular interaction and substituent effects exist, such as the introduction of electron-withdrawing groups to lower the LUMO energy [28]. Commonly used motives include the electron-rich D moieties thieno [3,4-*b*]thiophene (BDT), cyclopentadithiophene (CPDT) and dithieno [3,2-*b*:2′,3′-*d*]pyran (DTP), and the electron-poor A units diketopyrrolopyrrole (DPP), thienopyrzine (TP), benzothiadiazole (BT), and isoindigo (II) [28,30,46,47]. The synthetic strategies for narrow bandgap donor polymers are detailed further in the literature [29–31,38,48].

2.2. Narrow Band Gap Non-Fullerene Acceptors

To achieve highly transparent bulk-heterojunction photoactive layers and devices, a visibly transparent donor must be combined with an equally transparent acceptor molecule. Not only do the optical properties have to be matched with the donor, but a beneficial energy level alignment is necessary as well. Energetic offsets ($HOMO_D - HOMO_A$, ΔE_{HOMO}) should be minimized to reduce energetic losses E_{loss}, but need to be sufficiently high to guarantee efficient exciton dissociation at the interfaces of donor and acceptor rich domains [12,49–52]. State-of-the art non-fullerene acceptors (NFAs) are highly tunable on the molecular level, resulting in control over energy levels and optical properties, as well as morphological features, fulfilling the above-mentioned criteria with ease, in contrast to early generation fullerene acceptors. Current NFAs make use of established design concepts of earlier generation NFAs, such as (out-of-plane) side-chain engineering to control solubility and to prevent excessive aggregation behavior, and fused ring backbones to enhance π-π-stacking [53]. Vast progress in the reduction of the E_{loss} has been reported in the past years; while in 2018 E_{loss} <0.5 eV was considered low, now ultra-low losses of E_{loss} = 0.15 eV have been reported [13,54].

Similar to polymer donors, the alternation of donor and acceptor units (ADA type NFAs) was introduced in 2015 by Zhang et al. with the synthesis of ITIC, opening a platform for band gap engineering [55]. An efficient strategy to narrow the band gap in ADA type NFAs is to increase the electron-donating strength of the D core unit, for example by introducing carbon–oxygen-bridged (CO-bridged) latter type units. The oxygen atoms provide electron density and introduce planarity, which results in an extended π-conjugated system, narrowing the band gap further [56–58]. The introduction of π -bridges in A–π–D–π–A-type NFAs, is based on the same concept. Recent examples include the p-IO series by Lee et al. with band gaps between 1.34 eV and 1.20 eV, which can yield PCEs of up to 13.1% [59]. To date, the ultra-narrow band gap NFA COTIC-4F, a A-D′-D-D′-A type NFA that was reported in 2018 by Lee et al. remains the acceptor with the narrowest band gap reported [12]. Newer Y6 derivatives, so called A-DA′D-A NFAs, contain an electron-deficient core in the ladder-type fused rings and move towards equally narrow band gaps. Li et al. found in 2020 that when replacing the benzothiadiazole unit of Y6 with a benzotriazole unit, the electron-accepting ability of the triazole is reduced compared with that of the thiadiazole-based unit, leading to a narrower band gap of 1.38 eV instead of 1.40 Ev [21]. Hetero atom substitution with Se- or N-induced redshifted absorption by about 20 nm and 40 nm, respectively, extended it beyond 950 nm [13,60]. Lastly, insertion

of a double bond between the central core and the end groups to extend the conjugation lengths leads to a narrow optical band gap of 1.21 eV, as shown in 2021 by Jia et al [61]. The recent progress in Y-series acceptors promises the realization of novel NFAs with equally low or even lower band gaps in the future.

Figure 2A shows the achieved PCEs in dependence on the reported HOMO–LUMO gap of the used donor in combination with various acceptors and electrodes, Figure 2B depicts the same data for narrow NFAs. It is evident, that a large variety of NFA with band gaps E_g < 1.4 eV were synthesized in the years from 2017 until now. For donor polymers, we considered molecules with E_g < 1.6 eV. Although more donor examples with ultra-narrow band gaps of 1.0–1.2 eV exists, the achieved PCEs are limited. This explains why the vast majority of narrow band gap NFA reports rely on well-studied donor polymers, such as PTB7-Th, P3HT, PBDB-TF and PM6. Therefore, we conclude that currently narrow band gap polymers are performance-limiting components and suggest further exploration of high-performance narrow band gap polymer donor materials. A range of polymer donors and acceptors, sorted by their reported HOMO–LUMO gap, are shown in Figure 2C,D, respectively.

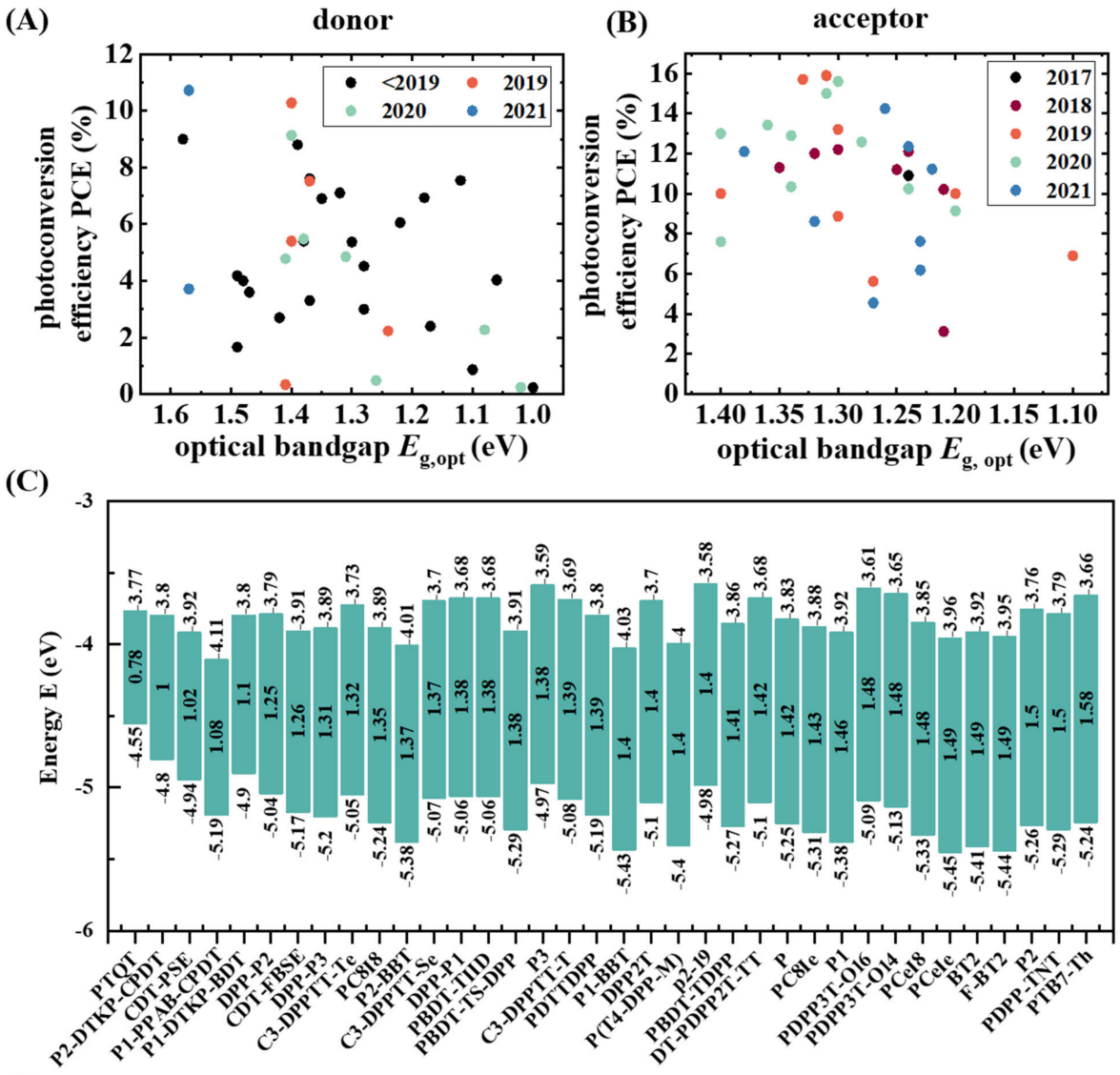

Figure 2. *Cont.*

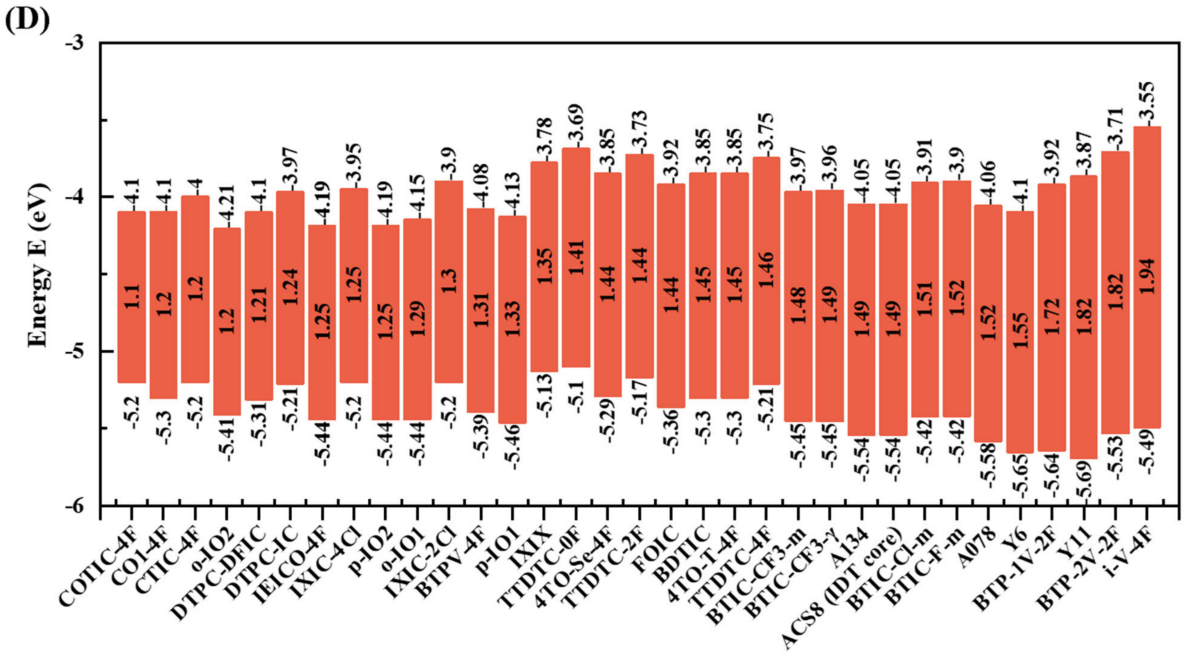

Figure 2. (**A**) PCE of OPVs in dependance on the band gap of the donor materials. (**B**) PCE of OPVs in dependance on the band gap of the acceptor materials. (**C**) Energy levels of donors, sorted by ascending band gap and labeled consistently with abbreviation in original publication. (**D**) Energy levels of acceptors, sorted by ascending band gap and labeled consistently with abbreviation in original publication.

3. Transparent Electrodes

Semitransparent solar cells require both front and back electrical contacts to be transparent in a wide UV–VIS–NIR spectral range while realizing an efficient collection of photo-generated charge carriers. Back transparent electrodes should be selected with the material features of organic semiconductors in mind. The sensitive nature of organic semiconductors restricts the deposition techniques of back electrodes onto active bulk-heterojunction layers. In particular, highly energetic magnetron sputtering may damage organic active layers even through very thin inorganic electron or hole transport layers [62].

Indium–Tin–Oxide (ITO) is the most common transparent conductive electrode material and typically used as front electrode material for ST-OPVs. Despite its widespread application, ITO electrodes have several disadvantages, which make the application of this material unfavorable for ST-OPVs. Drawbacks include the high price of indium and the possible degradation effects induced by diffusion of indium atoms. Another drawback of ITO electrodes is the relatively high absorption in the NIR region, the spectral region that is critically important for ST-OPVs that are based on IR-absorbing narrow band gap bulk-heterojunction active layers.

A cheaper alternative for ITO is fluorine-doped tin-oxide (FTO). FTO coatings offer a similar transparency with slightly lower electrical conductivity for a noticeably lower price than their ITO counterparts [63]. Moreover, the difference in the work functions of ITO (4.7 eV) and FTO (4.4 eV) typically does not influence the device performance due to the presence of electron (ZnO) or hole transport layers (PEDOT:PSS) for inverted or conventional device architectures, respectively.

Aydin et al. have shown that the relatively low transmittance of ITO in the NIR spectral region can be improved by the zirconium doping of indium oxide In_2O_3 [64]. Zr-doped indium oxide (IZRO) films possess low sheet resistance and exhibit high infrared transparency resulting in just 5% parasitic absorption of solar light in a wide spectral range from 250–2500 nm. These features make IZRO an excellentcandidate for the front electrodes of narrow band gap ST-OPVs.

MoOx(40 nm)/Au(10 nm)/MoOx(40 nm) electrodes were proposed as another alternative front electrode with higher transparency and even lower sheet resistance that can replace ITO [65].Electrodes comprising thin metal layers are also common back electrode candidates. The use of thin metal electrodes, such as 10 nm to 15 nm Ag, Au, or Al, often on top of an interlayer, such as MoOx, is one option for semitransparent back electrodes [18,66–68]. Simple processing and low cost are benefits of such electrodes. Thinner films generally exhibit higher resistivity because of electron scattering at the surface and grain boundaries, therefore, conductivity and transparency need to be balanced [67]. It is worth mentioning that for ultra-thin metal electrodes the change in the thickness-dependent electrical and optical properties of the metals need to be considered, the latter limiting the predictability of optical simulations, such as those carried out with Lumerical or transfer-matrix simulations. Additionally, the deposition technique and the film nucleation can impact the properties of the film, therefore, optical simulations should be carried out with much care and the optical simulation results should be interpreted with these considerations in mind. For example, the refractive index of Ag-thin films with thicknesses below 20nm shows significant thickness dependence and plasmonic effects. Plasmonic effects are specifically relevant for gold films [69–75].

In multi-layer oxide/metal/oxide electrodes, such as ZnO/Ag/IZO, GZO/Ag/GZO, ITO/Au/ITO, and MoO_3/Ag/MoO_3, the oxide layers increase the transmittance due to lower reflection at both metal interfaces and offer low resistance [76]. Grown via low-temperature reactive plasma deposition (RPD), the damaging effects can be minimized, as proposed by Zhang et al., that come with other oxide deposition methods, such as thermal evaporation, atomic layer deposition (ALD), and magnetron sputtering [76].

Transparent conductive back electrodes, based on solution-processed metal nanowires [77,78], transferred doped graphene [4,79], conducting polymers [80], or their hybrids [81–86] are currently promising in the field of organic semitransparent photovoltaics, offering mild processing conditions that are compatible with the organic active layer materials. These electrodes exhibit very high transmittance within a wide spectral range and suitably low sheet resistance [87–89]. Specifically, Ag nanowires are considered a favorable option due to their low sheet resistance, high optical transparency and mechanical flexibility, and solution processability that allows various processing methods, including printing methods or spray-coating. The remaining challenges are the high roughness of Ag nanowires, and agglomeration problems [80].

A general consideration about electrode requirements for semitransparent solar cells arises from the fact that ST-OPVs still generate lower photocurrents due to the utilization of only a fraction of the solar spectrum. Schopp et. al. have shown that strict requirements for the low series resistance of opaque solar cells become milder for their semitransparent counterparts [90]. Therefore, even untreated nanostructured electrodes with relatively high sheet resistance can be successfully implemented in semitransparent organic solar cells and a wider range of transparent electrode materials can be considered that are not suitable for opaque high-performance OPVs with high J_{sc} values.

4. Device Engineering

4.1. Evaluation of ST-OPVs: Figures of Merit

The average visible transmittance (AVT), also called average photopic transmittance (APT) or visible light transmittance (VLT), can be calculated from the spectral intensity distribution of the AM1.5 spectrum $I(\lambda)$ and the photopic spectral response of the human eye $V(\lambda)$, both shown in Figure 3A. The photopic response describes how the wavelength-dependent sensitivity of the eye under well-lit conditions ranges from about 370–740 nm, and peaks at 555 nm [91,92]. It is governed by the photosensitivity of three different types of photoreceptor cells, called cones, that sense red, green, and blue light.

$$\mathrm{AVT} = \mathrm{APT} = \mathrm{VLT} = \frac{\int I(\lambda) \cdot T(\lambda) \cdot V(\lambda)\, d\lambda}{\int T(\lambda) \cdot V(\lambda)\, d\lambda}$$

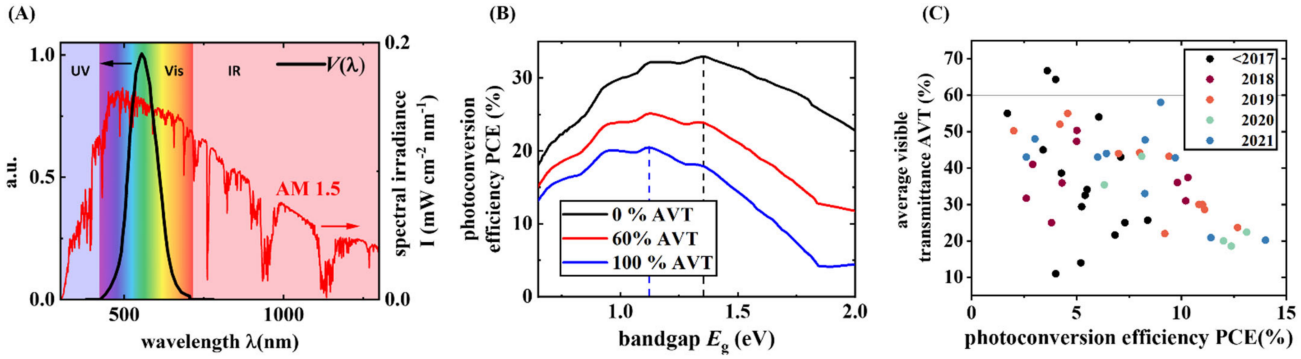

Figure 3. (**A**) Photopic response $V(\lambda)$ of the human eye (left axis) and solar irradiance of the AM1.5 spectrum (red, right axis). (**B**) Theoretical PCE limit of ST-OPV single-junctions in dependence on the band gap for different AVTs, illustrating the required shift to narrower band gaps for more transparent OPVs. (**C**) Relationship of the AVT and the PCE of ST-OPVs reported in the literature.

Another commonly reported figure of merit for ST-OPVs is the light utilization efficiency LUE. The LUE is the product of the PCE and the AVT.

$$\text{LUE} = \text{AVT} \cdot \text{PCE}$$

Taking into account both PCE and AVT, a direct comparison of LUE values can hold viable information in contrast to the direct comparison of the AVT values without knowledge of the PCE [93,94]. Another relevant factor for ST-OPVs is the color rendering index (CRI), ranging from 0 to 100. For most applications, high color neutrality is necessary, which means objects illuminated by light that has passed through an ST-OPV should appear to be of the same color as when illuminated by natural outdoor lighting [7,94]. As the standard reference for such conditions, the energy flux of the AM1.5 illumination is used in the field of ST-OPVs. High color neutrality is achieved by flat transmission spectra in the visible range and is not correlated with the AVT value. Details on the calculation can be found in the literature [94–96].

4.2. Theoretical Performance Limits of ST-OPVs

Before the development of narrow-band gap OPV materials, efforts were focused on ST-OPVs with thin active layers. Increased light absorption and photogeneration competed with the transparency, and thus low performances or low AVTs were reported [97]. With the development of narrow band gap materials, active layers with high photogeneration and high visible transparency have become reality due to efficient absorption in the IR-region of the spectrum. In fact, most of the solar energy is distributed in the IR region, resulting in higher theoretical performances for OPVs that exclusively absorb IR radiation compared to OPVs absorbing exclusively in the visible range [98]. The theoretical Shockley–Queisser (SQ) limit for visibly fully transparent OPVs is an impressive 20.6% when both UV and IR photons are harvested [99]. In this case, a narrow band gap of 1.12 eV is required and any deviations from this ideal band gap value lower the theoretical PCE limit, as can be seen in Figure 3B [93,99].

4.3. Current Performance and Strategies to Increase LUE

Most reported ST-OPVs have AVTs < 50% and PCEs in the wide range from 2–15%, as shown in Figure 3C. To date, only a few examples exist in the literature that demonstrate OPVs with AVTs exceeding 60%, and none of these show PCEs above 5%. Applications that require lower AVTs include gray privacy glass for automobile applications, with AVTs of only 18%, or tinted glass used in residential architecture to reduce solar heating, often having AVTs of 50–60% [100]. The most common applications, however, require higher AVTs of about 55%–90%; for example, regular monolithic glass windows that typically

transmit >90% of the light. A higher illuminance of indoor spaces not only saves energy due to reduced artificial lighting needs, but also plays a crucial role in the physical and mental wellbeing, productivity, and health of individuals [101]. Meeting the requirements for a high AVT remains, therefore, the main bottleneck for a widespread application of integrated ST-OPVs [53,97,100,102–104].

Several strategies exist to increase the LUE by either improving the AVT or the PCE without compromising the other. The PCE for example can be improved by incorporating a near-infrared distributed Bragg reflector (DBR), consisting of thin alternating layers of two materials with distinctly different refractive indices, such as TiO_2 and SiO_2 or LiF and MoO_3 [97,105]. The DBR allows the reflection of the IR back into the active layer to increase photon harvesting and the PCE. Li et al. placed a DBR behind a thin film Ag back electrode and demonstrated a concomitant reduction in the AVT upon the use of a DBR due to an observed shift of the device's transmission maximum to the response maximum of the human eye (555 nm) [106]. Similarly, aperiodic thin film coatings for ST-OPVs can help to achieve high neutral transmittance and an increased PCE by flattening the transmission spectrum and reflecting near IR photons [107].

Similarly, optical management layers can be deposited on top of the electrodes to increase the transparency of the device stack. Xie et al. reported highly transparent OPVs by fabricating a MoO_3/Ag/MoO_3 back electrode. Guided by optical simulations, an optimal capping layer thickness of 35 nm was found optimal to improve the AVT from 52% to 61.5% (PCE decreased from 4.2% to 3.5%) by increasing the transparency in the visible range from 500 nm to 800 nm, compared to the same device structure without the additional MoOx layer [108]. Li et al. recently reported ST-OPVs based on Glass/ITO/PEDOT:PSS/active layer/PFN-Br/Ag(13 nm) with and without a 50 nm thick high refractive index TeO_2 capping layer. The addition of the anti-reflective TeO_2 led to increased AVT from 30% to 50% while the PCE was only slightly reduced from 9.8% to 8.4% [109].

Li et al. successfully combined the above-mentioned strategies by using optical outcoupling and antireflection layers and a DBR to create a complex multi-layer device stack that enhances the transparency and increases cell absorption by enhancing IR back-reflection [110]. Their ternary cells comprising PCE10 and the two NFAs TT-FIC and BT-CIC reach an LUE of 3.56 $\pm$ 0.11%, a PCE of 8.0 $\pm$ 0.2%, and an APT of 44.2 $\pm$ 1.4%. The LUE is doubled, compared to ST-OPVs without the additional layers [110].

Beyond the engineering of the device stack and the incorporation of additional layers, the active layer transparency can be enhanced mainly by two approaches. First, a simple reduction in the active layer thickness can boost the AVT, however, typically at the high expense of a significantly reduced PCE. The exact impact of such a reduction, however, depends on the generation rate profile in the active layer. Typically, charge carrier generation rates are much higher near the front electrode–active layer interface and peak within the first few nanometers of the active layer.

Second, the *dilute donor approach* has been employed by several groups to improve as a platform for increasing the AVT while maintaining a high PCE due to increased IR absorption by a narrow band gap acceptor compound and reduced absorption by a donor compound that absorbs (partially) in the visible range [80,111–113]. In 2021, Yao et al. studied PM6:Y6 OPVs with reduced donor content and found an efficiency of over 10% in dilute donor solar cells with only 10 wt% PM6, thanks to efficient charge generation, electron and hole transport, slow charge recombination, and field-insensitive extraction [111]. Previously, Hu et al. reported cells with reduced relative donor content in 2019, improving the AVT of semitransparent ternary PTB7-Th:BDTThIT-4F:IECO-4F OPVs by decreasing the PTB7-Th content in active layers/increasing the near-IR NFA IEICO-4F content [114]. Similarly, Hu et al. reported ternary blends with an active layer AVT of 50.1%, leading to ST-OPVs with 20.2% and a PCE of 13.02% when employing D18-Cl:Y6-1O:Y6 in a 0.7:0.8:0.8 wt/wt ratio [111]. Xu et al. reported a PCE of 12.91% and an AVT of 22.49% with an excellent blend film AVT of over 50%, using the wide-band gap donor polymer D18 in combination with the near-IR absorbing N3 acceptor in 2021 in a dilute donor 0.7:1.6, wt/wt

ratio [115]. Highly diluted polymer donor chains may not form a percolating network for charge extraction, in contrast to the common morphological picture for BHJ solar cells. Theoretical and experimental work aims to explain successful photocurrent generation in such highly diluted donor (fullerene) OPVs with isolated donor molecules by a hole back-transfer mechanism that is dependent on the HOMO–HOMO offset between donor and acceptor [113,116,117].

5. Device Physics in Narrow Band Gap ST-OPVs

The understanding of the optoelectronic processes in NFA-based OPVs has been crucial to guide the development of next-generation OPVs. However, only a few works exist that address the inherent changes in the optoelectronic processes that are concomitant with increased transparency. As discussed in the above section on theoretical limitations, even fully transparent OPVs can absorb light in the UV or IR region to reach high theoretical PCEs of >20%. However, to date, the existing systems exhibit much lower performances due to lower absorption compared to their opaque counterparts, meaning that fewer charge carriers are photogenerated in the active layers of ST-OPVs compared to high-performance state-of-the-art OPVs. This reduction in the generation rate can originate from low absorption coefficients of the active layer compounds in the visible range and is enhanced when thin active layers are employed and when the back-electrode reflection is purposefully minimized to reach higher AVTs. As Schopp et al. have derived, this reduction in the generation rate and short-circuit current can be counteracted to a small degree by increases in the extraction efficiency with the AVT [90].

5.1. Changes in Active Layer-Importance of Bulk Recombination and Shunt Leakage

Concomitant with the reduced photogeneration is a reduced J_{sc} and V_{oc}. However, more complex changes are inherent to more transparent devices than the mere reduction in the performance parameters. Based on a narrow band gap model BHJ active layers with systematically varied transparency in the visible range, Schopp et al. were able to show inherent changes in the recombination dynamics upon increased transparency [90]. Charge carriers can recombine from band-to-band (bimolecular recombination), or via traps. The latter can be subdivided into bulk trap-assisted recombination and surface trap-assisted recombination contributions arising from the active layer interfaces [118–123].

Their modeling work shows that with increased AVT the importance of bulk-trap assisted recombination increases. This is seen from increased V_{oc}-ln$I$ slopes and further confirmed by an increased relative recombination contribution via bulk traps [90]. In contrast, the relative bimolecular recombination contributions were shown to be slightly reduced and surface trap-assisted recombination decreased significantly upon increasing the AVT of the active layer materials when maintaining all other material and device parameters constant. Figure 4A illustrates these changes in the recombination rates and Figure 4B shows the change in their relative contribution with increased AVT. Schopp et al.'s findings highlight that high-purity and morphologically optimized active layers with low trap density are required for ST-OPVs based on near-IR materials [90].

However, when comparing two hypothetical wide and narrow band gap systems with the same charge carrier densities, the effect of bulk trap-assisted recombination will be less detrimental in the narrow band gap OPV, as Brus et al. have shown that the relative contribution of the trap-assisted recombination in organic BHJ active layers increases with their effective band gap [124]. This is caused by a lower probability of forming deep defect/impurity energy levels and more favorable band-to-band transitions in narrow band gap semiconductors.

Besides bulk trap-assisted recombination, leakage pathways in the active layer can be an additional loss contribution, which can lead to decreased V_{oc}. Schopp et al. pointed out that transparent devices are more sensitive to shunt-leakage, which emphasizes the need for high-quality active layers even more.

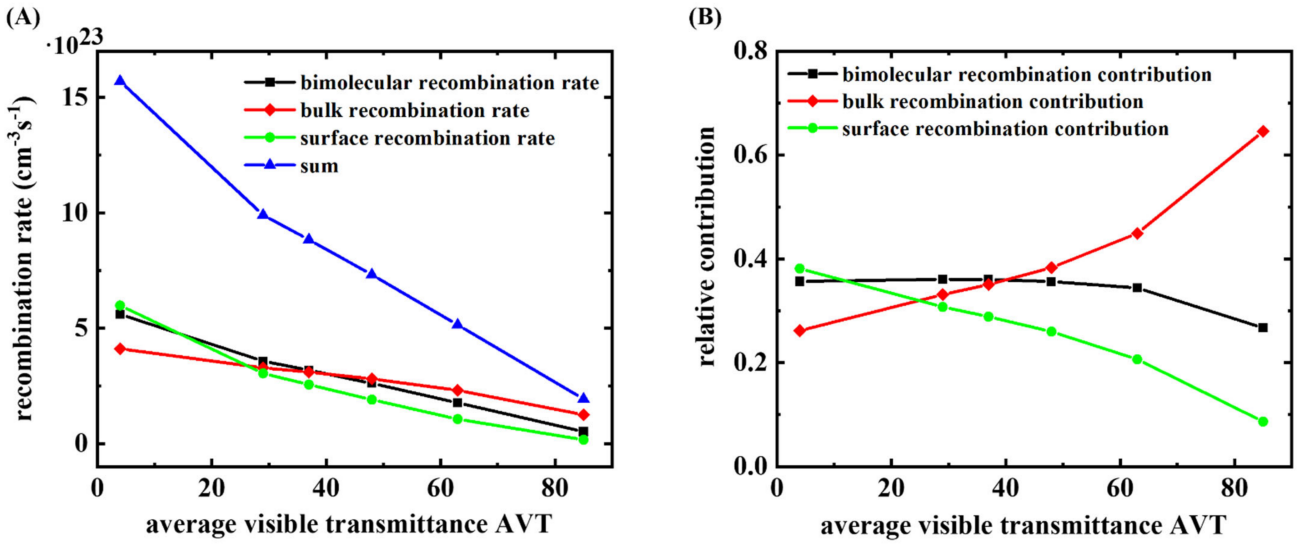

Figure 4. (**A**) Recombination rates in dependence on the AVT of the device stack and (**B**) the relative recombination contributions of the different recombination channels.

5.2. Changes in the Interfacial Processes in Narrow Band Gap OPVs

Non-ohmic contacts, poor interfacial optimization, and mechanical bending can give rise to high series resistance and reduced J_{sc}. With an increase in transparency, Schopp et al. have demonstrated that the negative effect of the series resistance is less relevant than in opaque devices. Therefore, a wider range of transparent electrodes and flexible device architectures can be considered a suitable choice for ST-OPVs [90]. Another aspect to consider for narrow band gap near-IR absorbing ST-OPV blends is the shifted absorption and its implications for the back electrode material choice. Thin metal films, a common electrode option, vary in their optical properties and their ability to reflect in the near-IR region. Schopp et al. have demonstrated, that the ideal electrode choice depends on the absorber band gap and the thickness of the active layer. Many opaque systems rely on Ag electrodes, whereas a change to Au electrodes for thin narrow-band gap active layers can boost the performance [125].

6. Conclusions

In this review, we have given an overview of the current ST-OPV landscape. Various strategies to improve the AVT of ST-OPVs are outlined, addressing the photoactive blend, as well as the whole device stack. Synthetic strategies, such as quinoid stabilization or D:A alteration, are discussed and a wide range of narrow bandgap donor and acceptor molecules are presented, illustrating a need for new narrow bandgap donor materials. Moreover, semitransparent electrode materials are reviewed, including common choices, such as nanowires, thin metal electrodes, or multi-layer structures, alongside engineering approaches to improve the AVT while maintaining high PCEs.

A comparison of current PCEs with theoretical limitations demonstrated that while the donor–acceptor material and electrode design is progressing rapidly, the discrepancy between the current performances and the theoretical limitations remains large. To narrow the current gap, fundamental device physics considerations should be taken into account to guide the design of ST-OPVs. For example, high-purity and morphologically optimized active layers with low trap density are required due to the increased importance of bulk traps in ST-OPVs. Further research aiming to create a better understanding of the requirements for ST-OPVs and how they differ from traditional opaque devices in the photoelectronic processes, as well as applied research promoting the material development specifically on the donor side, are expected to move the field forward quickly.

Author Contributions: V.V.B. and N.S. drafted the concept of the manuscript. N.S. collected data from literature, drafted the manuscript and prepared figures. V.V.B. provided feedback and revision suggestions for the manuscript and drafted the section about transparent electrodes. All authors have read and agreed to the published version of the manuscript.

Funding: Faculty-Development Competitive Research Program Grant of Nazarbayev University (11022021FD2915), Link Foundation (Link Energy Fellowship).

Institutional Review Board Statement: Not applicable.

Informed Consent Statement: Not applicable.

Acknowledgments: The authors thank Dylan Choi for help with generating chemical structures in ChemDraw.

Conflicts of Interest: The authors declare no conflict of interest.

References

1. Ajayan, J.; Nirmal, D.; Mohankumar, P.; Saravanan, M.; Jagadesh, M.; Arivazhagan, L. A Review of Photovoltaic Performance of Organic/Inorganic Solar Cells for Future Renewable and Sustainable Energy Technologies. *Superlattices Microstruct.* **2020**, *143*, 106549. [CrossRef]
2. Brabec, C.J.; Distler, A.; Du, X.; Egelhaaf, H.-J.; Hauch, J.; Heumueller, T.; Li, N. Material Strategies to Accelerate OPV Technology Toward a GW Technology. *Adv. Energy Mater.* **2020**, *10*, 2001864. [CrossRef]
3. Husain, A.A.F.; Hasan, W.Z.W.; Shafie, S.; Hamidon, M.N.; Pandey, S.S. A Review of Transparent Solar Photovoltaic Technologies. *Renew. Sustain. Energy Rev.* **2018**, *94*, 779–791. [CrossRef]
4. Shin, D.H.; Jang, C.W.; Lee, H.S.; Seo, S.W.; Choi, S.-H. Semitransparent Flexible Organic Solar Cells Employing Doped-Graphene Layers as Anode and Cathode Electrodes. *ACS Appl. Mater. Interfaces* **2018**, *10*, 3596–3601. [CrossRef]
5. Li, Y.; Xu, G.; Cui, C.; Li, Y. Flexible and Semitransparent Organic Solar Cells. *Adv. Energy Mater.* **2018**, *8*, 1701791. [CrossRef]
6. Kaltenbrunner, M.; White, M.S.; Głowacki, E.D.; Sekitani, T.; Someya, T.; Sariciftci, N.S.; Bauer, S. Ultrathin and Lightweight Organic Solar Cells with High Flexibility. *Nat. Commun.* **2012**, *3*, 770. [CrossRef]
7. Brus, V.V.; Lee, J.; Luginbuhl, B.R.; Ko, S.-J.; Bazan, G.C.; Nguyen, T.-Q. Hall of Fame Article: Solution-Processed Semitransparent Organic Photovoltaics: From Molecular Design to Device Performance (Adv. Mater. 30/2019). *Adv. Mater.* **2019**, *31*, 1970219. [CrossRef]
8. Aghassi, A.; Fay, C.D. Understanding the Loss Mechanisms in High-Performance Solution-Processed Small Molecule Bulk Heterojunction Solar Cells Doped with a PFN Impurity. *Phys. Chem. Chem. Phys.* **2019**, *21*, 13176–13185. [CrossRef]
9. Krebs, F.C. Fabrication and Processing of Polymer Solar Cells: A Review of Printing and Coating Techniques. *Sol. Energy Mater. Sol. Cells* **2009**, *93*, 394–412. [CrossRef]
10. Admassie, S.; Inganäs, O.; Mammo, W.; Perzon, E.; Andersson, M.R. Electrochemical and Optical Studies of the Band Gaps of Alternating Polyfluorene Copolymers. *Synth. Met.* **2006**, *156*, 614–623. [CrossRef]
11. Phan, H.; Kelly, T.J.; Zhugayevych, A.; Bazan, G.C.; Nguyen, T.-Q.; Jarvis, E.A.; Tretiak, S. Tuning Optical Properties of Conjugated Molecules by Lewis Acids: Insights from Electronic Structure Modeling. *J. Phys. Chem. Lett.* **2019**, *10*, 4632–4638. [CrossRef]
12. Lee, J.; Ko, S.-J.; Seifrid, M.; Lee, H.; Luginbuhl, B.R.; Karki, A.; Ford, M.; Rosenthal, K.; Cho, K.; Nguyen, T.-Q.; et al. Bandgap Narrowing in Non-Fullerene Acceptors: Single Atom Substitution Leads to High Optoelectronic Response Beyond 1000 Nm. *Adv. Energy Mater.* **2018**, *8*, 1801212. [CrossRef]
13. Liu, W.; Sun, S.; Zhou, L.; Cui, Y.; Zhang, W.; Hou, J.; Liu, F.; Xu, S.; Zhu, X. Design of Near-Infrared Nonfullerene Acceptor with Ultralow Nonradiative Voltage Loss for High-Performance Semitransparent Ternary Organic Solar Cells. *Angew. Chem. Int. Ed.* **2022**, *61*, e202116111. [CrossRef]
14. Anctil, A.; Lee, E.; Lunt, R.R. Net Energy and Cost Benefit of Transparent Organic Solar Cells in Building-Integrated Applications. *Appl. Energy* **2020**, *261*, 114429. [CrossRef]
15. Ballif, C.; Perret-Aebi, L.-E.; Lufkin, S.; Rey, E. Integrated Thinking for Photovoltaics in Buildings. *Nat. Energy* **2018**, *3*, 438. [CrossRef]
16. Jelle, B.P.; Breivik, C. State-of-the-Art Building Integrated Photovoltaics. *Energy Procedia* **2012**, *20*, 68–77. [CrossRef]
17. Jelle, B.P.; Breivik, C. The Path to the Building Integrated Photovoltaics of Tomorrow. *Energy Procedia* **2012**, *20*, 78–87. [CrossRef]
18. Li, Y.; Guo, X.; Peng, Z.; Qu, B.; Yan, H.; Ade, H.; Zhang, M.; Forrest, S.R. Color-Neutral, Semitransparent Organic Photovoltaics for Power Window Applications. *Proc. Natl. Acad. Sci. USA* **2020**, *117*, 21147–21154. [CrossRef]
19. Yuan, J.; Zhang, Y.; Zhou, L.; Zhang, G.; Yip, H.-L.; Lau, T.-K.; Lu, X.; Zhu, C.; Peng, H.; Johnson, P.A.; et al. Single-Junction Organic Solar Cell with over 15% Efficiency Using Fused-Ring Acceptor with Electron-Deficient Core. *Joule* **2019**, *3*, 1140–1151. [CrossRef]
20. Karki, A.; Vollbrecht, J.; Dixon, A.L.; Schopp, N.; Schrock, M.; Reddy, G.N.M.; Nguyen, T.-Q. Understanding the High Performance of over 15% Efficiency in Single-Junction Bulk Heterojunction Organic Solar Cells. *Adv. Mater.* **2019**, *31*, 1903868. [CrossRef]

21. Zhu, C.; Yuan, J.; Cai, F.; Meng, L.; Zhang, H.; Chen, H.; Li, J.; Qiu, B.; Peng, H.; Chen, S.; et al. Tuning the Electron-Deficient Core of a Non-Fullerene Acceptor to Achieve over 17% Efficiency in a Single-Junction Organic Solar Cell. *Energy Environ. Sci.* **2020**, *13*, 2459–2466. [CrossRef]
22. Fan, B.; Zhang, D.; Li, M.; Zhong, W.; Zeng, Z.; Ying, L.; Huang, F.; Cao, Y. Achieving over 16% Efficiency for Single-Junction Organic Solar Cells. *Sci. China Chem.* **2019**, *62*, 746–752. [CrossRef]
23. Cui, Y.; Yao, H.; Zhang, J.; Zhang, T.; Wang, Y.; Hong, L.; Xian, K.; Xu, B.; Zhang, S.; Peng, J.; et al. Over 16% Efficiency Organic Photovoltaic Cells Enabled by a Chlorinated Acceptor with Increased Open-Circuit Voltages. *Nat. Commun.* **2019**, *10*, 2515. [CrossRef]
24. Gutzler, R.; Perepichka, D.F. π-Electron Conjugation in Two Dimensions. *J. Am. Chem. Soc.* **2013**, *135*, 16585–16594. [CrossRef]
25. Gutzler, R. Band-Structure Engineering in Conjugated 2D Polymers. *Phys. Chem. Chem. Phys.* **2016**, *18*, 29092–29100. [CrossRef]
26. Scharber, M.C.; Sariciftci, N.S. Low Band Gap Conjugated Semiconducting Polymers. *Adv. Mater. Technol.* **2021**, *6*, 2000857. [CrossRef]
27. Liu, X.; Sun, Y.; Hsu, B.B.Y.; Lorbach, A.; Qi, L.; Heeger, A.J.; Bazan, G.C. Design and Properties of Intermediate-Sized Narrow Band-Gap Conjugated Molecules Relevant to Solution-Processed Organic Solar Cells. *J. Am. Chem. Soc.* **2014**, *136*, 5697–5708. [CrossRef]
28. Liu, C.; Wang, K.; Gong, X.; Heeger, A.J. Low Bandgap Semiconducting Polymers for Polymeric Photovoltaics. *Chem. Soc. Rev.* **2016**, *45*, 4825–4846. [CrossRef]
29. Cheng, Y.-J.; Yang, S.-H.; Hsu, C.-S. Synthesis of Conjugated Polymers for Organic Solar Cell Applications. *Chem. Rev.* **2009**, *109*, 5868–5923. [CrossRef]
30. Dou, L.; Liu, Y.; Hong, Z.; Li, G.; Yang, Y. Low-Bandgap Near-IR Conjugated Polymers/Molecules for Organic Electronics. *Chem. Rev.* **2015**, *115*, 12633–12665. [CrossRef]
31. Lim, D.-H.; Ha, J.-W.; Choi, H.; Cheol Yoon, S.; Ram Lee, B.; Ko, S.-J. Recent Progress of Ultra-Narrow-Bandgap Polymer Donors for NIR-Absorbing Organic Solar Cells. *Nanoscale Adv.* **2021**, *3*, 4306–4320. [CrossRef]
32. Kitamura, C.; Tanaka, S.; Yamashita, Y. Design of Narrow-Bandgap Polymers. Syntheses and Properties of Monomers and Polymers Containing Aromatic-Donor and o-Quinoid-Acceptor Units. *Chem. Mater.* **1996**, *8*, 570–578. [CrossRef]
33. Lee, Y.S.; Kertesz, M. The effect of additional fused rings on the stabilities and the band gaps of heteroconjugated polymers. *Int. J. Quantum Chem.* **1987**, *32*, 163–170. [CrossRef]
34. Wudl, F.; Kobayashi, M.; Heeger, A.J. Poly(Isothianaphthene). *J. Org. Chem.* **1984**, *49*, 3382–3384. [CrossRef]
35. Brédas, J.L.; Heeger, A.J.; Wudl, F. Towards Organic Polymers with Very Small Intrinsic Band Gaps. I. Electronic Structure of Polyisothianaphthene and Derivatives. *J. Chem. Phys.* **1986**, *85*, 4673–4678. [CrossRef]
36. Kawabata, K.; Saito, M.; Osaka, I.; Takimiya, K. Very Small Bandgap π-Conjugated Polymers with Extended Thienoquinoids. *J. Am. Chem. Soc.* **2016**, *138*, 7725–7732. [CrossRef]
37. Steckler, T.T.; Henriksson, P.; Mollinger, S.; Lundin, A.; Salleo, A.; Andersson, M.R. Very Low Band Gap Thiadiazoloquinoxaline Donor–Acceptor Polymers as Multi-Tool Conjugated Polymers. *J. Am. Chem. Soc.* **2014**, *136*, 1190–1193. [CrossRef]
38. Mikie, T.; Osaka, I. Small-Bandgap Quinoid-Based π-Conjugated Polymers. *J. Mater. Chem. C* **2020**, *8*, 14262–14288. [CrossRef]
39. Li, X.; Guo, J.; Yang, L.; Chao, M.; Zheng, L.; Ma, Z.; Hu, Y.; Zhao, Y.; Chen, H.; Liu, Y. Low Bandgap Donor-Acceptor π-Conjugated Polymers From Diarylcyclopentadienone-Fused Naphthalimides. *Front. Chem.* **2019**, *7*, 362. [CrossRef]
40. Wardani, R.P.; Jeong, M.; Lee, S.W.; Whang, D.R.; Kim, J.H.; Chang, D.W. Simple Methoxy-Substituted Quinoxaline-Based D-A Type Polymers for Nonfullerene Polymer Solar Cells. *Dye. Pigment.* **2021**, *192*, 109346. [CrossRef]
41. Yue, H.; Kong, L.; Wang, B.; Yuan, Q.; Zhang, Y.; Du, H.; Dong, Y.; Zhao, J. Synthesis and Characterization of Novel D-A Type Neutral Blue Electrochromic Polymers Containing Pyrrole [3-c]Pyrrole-1,4-Diketone as the Acceptor Units and the Aromatics Donor Units with Different Planar Structures. *Polymers* **2019**, *11*, 2023. [CrossRef]
42. Nakashima, M.; Otsura, T.; Naito, H.; Ohshita, J. Synthesis of New D-A Polymers Containing Disilanobithiophene Donor and Application to Bulk Heterojunction Polymer Solar Cells. *Polym. J.* **2015**, *47*, 733–738. [CrossRef]
43. Murugesan, V.; de Bettignies, R.; Mercier, R.; Guillerez, S.; Perrin, L. Synthesis and Characterizations of Benzotriazole Based Donor–Acceptor Copolymers for Organic Photovoltaic Applications. *Synth. Met.* **2012**, *162*, 1037–1045. [CrossRef]
44. Hückel, E. Zur Quantentheorie der Doppelbindung. *Z. Phys.* **1930**, *60*, 423–456. [CrossRef]
45. Slifkin, M.A. Molecular Orbital Theory and Experimentally Determined Energy-Levels. *Nature* **1963**, *200*, 877–879. [CrossRef]
46. Kim, J.; Hong, Z.; Li, G.; Song, T.; Chey, J.; Lee, Y.S.; You, J.; Chen, C.-C.; Sadana, D.K.; Yang, Y. 10.5% Efficient Polymer and Amorphous Silicon Hybrid Tandem Photovoltaic Cell. *Nat. Commun.* **2015**, *6*, 6391. [CrossRef]
47. Dou, L.; Chen, C.-C.; Yoshimura, K.; Ohya, K.; Chang, W.-H.; Gao, J.; Liu, Y.; Richard, E.; Yang, Y. Synthesis of 5H-Dithieno [3,2-b:2′,3′-d]Pyran as an Electron-Rich Building Block for Donor–Acceptor Type Low-Bandgap Polymers. *Macromolecules* **2013**, *46*, 3384–3390. [CrossRef]
48. Cheng, P.; Yang, Y. Narrowing the Band Gap: The Key to High-Performance Organic Photovoltaics. *Acc. Chem. Res.* **2020**, *53*, 1218–1228. [CrossRef]
49. Yang, C.; Zhang, J.; Liang, N.; Yao, H.; Wei, Z.; He, C.; Yuan, X.; Hou, J. Effects of Energy-Level Offset between a Donor and Acceptor on the Photovoltaic Performance of Non-Fullerene Organic Solar Cells. *J. Mater. Chem. A* **2019**, *7*, 18889–18897. [CrossRef]

50. Karki, A.; Vollbrecht, J.; Gillett, A.J.; Selter, P.; Lee, J.; Peng, Z.; Schopp, N.; Dixon, A.L.; Schrock, M.; Nádaždy, V.; et al. Unifying Charge Generation, Recombination, and Extraction in Low-Offset Non-Fullerene Acceptor Organic Solar Cells. *Adv. Energy Mater.* **2020**, *10*, 2001203. [CrossRef]
51. Zhang, J.; Liu, W.; Zhang, M.; Liu, Y.; Zhou, G.; Xu, S.; Zhang, F.; Zhu, H.; Liu, F.; Zhu, X. Revealing the Critical Role of the HOMO Alignment on Maximizing Current Extraction and Suppressing Energy Loss in Organic Solar Cells. *iScience* **2019**, *19*, 883–893. [CrossRef]
52. Ran, N.A.; Love, J.A.; Heiber, M.C.; Jiao, X.; Hughes, M.P.; Karki, A.; Wang, M.; Brus, V.V.; Wang, H.; Neher, D.; et al. Charge Generation and Recombination in an Organic Solar Cell with Low Energetic Offsets. *Adv. Energy Mater.* **2018**, *8*, 1701073. [CrossRef]
53. Armin, A.; Li, W.; Sandberg, O.J.; Xiao, Z.; Ding, L.; Nelson, J.; Neher, D.; Vandewal, K.; Shoaee, S.; Wang, T.; et al. A History and Perspective of Non-Fullerene Electron Acceptors for Organic Solar Cells. *Adv. Energy Mater.* **2021**, *11*, 2003570. [CrossRef]
54. Wang, J.; Xie, S.; Zhang, D.; Wang, R.; Zheng, Z.; Zhou, H.; Zhang, Y. Ultra-Narrow Bandgap Non-Fullerene Organic Solar Cells with Low Voltage Losses and a Large Photocurrent. *J. Mater. Chem. A* **2018**, *6*, 19934–19940. [CrossRef]
55. Lin, Y.; Wang, J.; Zhang, Z.-G.; Bai, H.; Li, Y.; Zhu, D.; Zhan, X. An Electron Acceptor Challenging Fullerenes for Efficient Polymer Solar Cells. *Adv. Mater.* **2015**, *27*, 1170–1174. [CrossRef]
56. Xiao, Z.; Liu, F.; Geng, X.; Zhang, J.; Wang, S.; Xie, Y.; Li, Z.; Yang, H.; Yuan, Y.; Ding, L. A Carbon-Oxygen-Bridged Ladder-Type Building Block for Efficient Donor and Acceptor Materials Used in Organic Solar Cells. *Sci. Bull.* **2017**, *62*, 1331–1336. [CrossRef]
57. Xiao, Z.; Jia, X.; Li, D.; Wang, S.; Geng, X.; Liu, F.; Chen, J.; Yang, S.; Russell, T.P.; Ding, L. 26 mA cm−2Jsc from Organic Solar Cells with a Low-Bandgap Nonfullerene Acceptor. *Sci. Bull.* **2017**, *62*, 1494–1496. [CrossRef]
58. Li, H.; Xiao, Z.; Ding, L.; Wang, J. Thermostable Single-Junction Organic Solar Cells with a Power Conversion Efficiency of 14.62%. *Sci. Bull.* **2018**, *63*, 340–342. [CrossRef]
59. Lee, J.; Song, S.; Huang, J.; Du, Z.; Lee, H.; Zhu, Z.; Ko, S.-J.; Nguyen, T.-Q.; Kim, J.Y.; Cho, K.; et al. Bandgap Tailored Nonfullerene Acceptors for Low-Energy-Loss Near-Infrared Organic Photovoltaics. *ACS Mater. Lett.* **2020**, *2*, 395–402. [CrossRef]
60. Yang, C.; An, Q.; Bai, H.-R.; Zhi, H.-F.; Ryu, H.S.; Mahmood, A.; Zhao, X.; Zhang, S.; Woo, H.Y.; Wang, J.-L. A Synergistic Strategy of Manipulating the Number of Selenophene Units and Dissymmetric Central Core of Small Molecular Acceptors Enables Polymer Solar Cells with 17.5% Efficiency. *Angew. Chem. Int. Ed.* **2021**, *60*, 19241–19252. [CrossRef]
61. Jia, Z.; Qin, S.; Meng, L.; Ma, Q.; Angunawela, I.; Zhang, J.; Li, X.; He, Y.; Lai, W.; Li, N.; et al. High Performance Tandem Organic Solar Cells via a Strongly Infrared-Absorbing Narrow Bandgap Acceptor. *Nat. Commun.* **2021**, *12*, 178. [CrossRef]
62. Ahlswede, E.; Hanisch, J.; Powalla, M. Influence of Cathode Sputter Deposition on Organic Solar Cells. *Appl. Phys. Lett.* **2007**, *90*, 063513. [CrossRef]
63. Way, A.; Luke, J.; Evans, A.D.; Li, Z.; Kim, J.-S.; Durrant, J.R.; Hin Lee, H.K.; Tsoi, W.C. Fluorine Doped Tin Oxide as an Alternative of Indium Tin Oxide for Bottom Electrode of Semi-Transparent Organic Photovoltaic Devices. *AIP Adv.* **2019**, *9*, 085220. [CrossRef]
64. Aydin, E.; De Bastiani, M.; Yang, X.; Sajjad, M.; Aljamaan, F.; Smirnov, Y.; Hedhili, M.N.; Liu, W.; Allen, T.G.; Xu, L.; et al. Zr-Doped Indium Oxide (IZRO) Transparent Electrodes for Perovskite-Based Tandem Solar Cells. *Adv. Funct. Mater.* **2019**, *29*, 1901741. [CrossRef]
65. Kim, M.; Lim, C.; Jeong, D.; Nam, H.-S.; Kim, J.; Lee, J. Design of a MoOx/Au/MoOx Transparent Electrode for High-Performance OLEDs. *Org. Electron.* **2016**, *36*, 61–67. [CrossRef]
66. Lee, K.-S.; Kim, I.; Yeon, C.B.; Lim, J.W.; Yun, S.J.; Jabbour, G.E. Thin Metal Electrodes for Semitransparent Organic Photovoltaics. *ETRI J.* **2013**, *35*, 587–593. [CrossRef]
67. O'Connor, B.; Haughn, C.; An, K.-H.; Pipe, K.P.; Shtein, M. Transparent and Conductive Electrodes Based on Unpatterned, Thin Metal Films. *Appl. Phys. Lett.* **2008**, *93*, 223304. [CrossRef]
68. Chen, K.-S.; Salinas, J.-F.; Yip, H.-L.; Huo, L.; Hou, J.; Jen, A.K.-Y. Semi-Transparent Polymer Solar Cells with 6% PCE, 25% Average Visible Transmittance and a Color Rendering Index Close to 100 for Power Generating Window Applications. *Energy Environ. Sci.* **2012**, *5*, 9551. [CrossRef]
69. Sun, X.; Hong, R.; Hou, H.; Fan, Z.; Shao, J. Thickness Dependence of Structure and Optical Properties of Silver Films Deposited by Magnetron Sputtering. *Thin Solid Films* **2007**, *515*, 6962–6966. [CrossRef]
70. Hövel, M.; Gompf, B.; Dressel, M. Dielectric Properties of Ultrathin Metal Films around the Percolation Threshold. *Phys. Rev. B* **2010**, *81*, 035402. [CrossRef]
71. Derkachova, A.; Kolwas, K.; Demchenko, I. Dielectric Function for Gold in Plasmonics Applications: Size Dependence of Plasmon Resonance Frequencies and Damping Rates for Nanospheres. *Plasmonics* **2016**, *11*, 941–951. [CrossRef]
72. Ghosh, P.K.; Debu, D.T.; French, D.A.; Herzog, J.B. Calculated Thickness Dependent Plasmonic Properties of Gold Nanobars in the Visible to Near-Infrared Light Regime. *PLoS ONE* **2017**, *12*, e0177463. [CrossRef]
73. McPeak, K.M.; Jayanti, S.V.; Kress, S.J.P.; Meyer, S.; Iotti, S.; Rossinelli, A.; Norris, D.J. Plasmonic Films Can Easily Be Better: Rules and Recipes. *ACS Photonics* **2015**, *2*, 326–333. [CrossRef]
74. Gordel, M.; Olesiak-Banska, J.; Kolkowski, R.; Matczyszyn, K.; Buckle, M.; Samoc, M. Shell-Thickness-Dependent Nonlinear Optical Properties of Colloidal Gold Nanoshells. *J. Mater. Chem. C* **2014**, *2*, 7239–7246. [CrossRef]
75. Ji, C.; Liu, D.; Zhang, C.; Jay Guo, L. Ultrathin-Metal-Film-Based Transparent Electrodes with Relative Transmittance Surpassing 100%. *Nat. Commun.* **2020**, *11*, 3367. [CrossRef]

76. Zhang, Y.; Liu, Z.; Ji, C.; Chen, X.; Hou, G.; Li, Y.; Zhou, X.; Cui, X.; Yang, X.; Ren, C.; et al. Low-Temperature Oxide/Metal/Oxide Multilayer Films as Highly Transparent Conductive Electrodes for Optoelectronic Devices. *ACS Appl. Energy Mater.* **2021**, *4*, 6553–6561. [CrossRef]
77. Yang, Y.; Xu, B.; Hou, J. Solution-Processed Silver Nanowire as Flexible Transparent Electrodes in Organic Solar Cells. *Chin. J. Chem.* **2021**, *39*, 2315–2329. [CrossRef]
78. Tam, K.C.; Kubis, P.; Maisch, P.; Brabec, C.J.; Egelhaaf, H.-J. Fully Printed Organic Solar Modules with Bottom and Top Silver Nanowire Electrodes. *Prog. Photovolt. Res. Appl.* **2022**, *30*, 528–542. [CrossRef]
79. Velasco Davoise, L.; Díez-Pascual, A.M.; Peña Capilla, R. Application of Graphene-Related Materials in Organic Solar Cells. *Materials* **2022**, *15*, 1171. [CrossRef]
80. Yao, N.; Xia, Y.; Liu, Y.; Chen, S.; Jonsson, M.P.; Zhang, F. Solution-Processed Highly Efficient Semitransparent Organic Solar Cells with Low Donor Contents. *ACS Appl. Energy Mater.* **2021**, *4*, 14335–14341. [CrossRef]
81. Wan, X.; Long, G.; Huang, L.; Chen, Y. Graphene—A Promising Material for Organic Photovoltaic Cells. *Adv. Mater.* **2011**, *23*, 5342–5358. [CrossRef]
82. Zhang, Q.; Wan, X.; Xing, F.; Huang, L.; Long, G.; Yi, N.; Ni, W.; Liu, Z.; Tian, J.; Chen, Y. Solution-Processable Graphene Mesh Transparent Electrodes for Organic Solar Cells. *Nano Res.* **2013**, *6*, 478–484. [CrossRef]
83. Shin, S.; Kim, J.; Kim, Y.-H.; Kim, S.-I. Enhanced Performance of Organic Light-Emitting Diodes by Using Hybrid Anodes Composed of Graphene and Conducting Polymer. *Curr. Appl. Phys.* **2013**, *13*, S144–S147. [CrossRef]
84. Dianetti, M.; Susanna, G.; Calabrò, E.; Polino, G.; Otto, M.; Neumaier, D.; Reale, A.; Brunetti, F. Graphene with Ni-Grid as Semitransparent Electrode for Bulk Heterojunction Solar Cells (BHJ-SCs). *Polymers* **2022**, *14*, 1046. [CrossRef]
85. Cui, N.; Song, Y.; Tan, C.-H.; Zhang, K.; Yang, X.; Dong, S.; Xie, B.; Huang, F. Stretchable Transparent Electrodes for Conformable Wearable Organic Photovoltaic Devices. *npj Flex. Electron.* **2021**, *5*, 31. [CrossRef]
86. Sagadevan, S.; Shahid, M.M.; Yiqiang, Z.; Oh, W.-C.; Soga, T.; Lett, J.A.; Alshahateet, S.F.; Fatimah, I.; Waqar, A.; Paiman, S.; et al. Functionalized Graphene-Based Nanocomposites for Smart Optoelectronic Applications. *Nanotechnol. Rev.* **2021**, *10*, 605–635. [CrossRef]
87. Morales-Masis, M.; De Wolf, S.; Woods-Robinson, R.; Ager, J.W.; Ballif, C. Transparent Electrodes for Efficient Optoelectronics. *Adv. Electron. Mater.* **2017**, *3*, 1600529. [CrossRef]
88. Brus, V.V.; Gluba, M.A.; Mai, C.-K.; Fronk, S.L.; Rappich, J.; Nickel, N.H.; Bazan, G.C. Conjugated Polyelectrolyte/Graphene Hetero-Bilayer Nanocomposites Exhibit Temperature Switchable Type of Conductivity. *Adv. Electron. Mater.* **2017**, *3*, 1600515. [CrossRef]
89. Kaikanov, M.; Kemelbay, A.; Amanzhulov, B.; Demeuova, G.; Akhtanova, G.; Bozheyev, F.; Tikhonov, A. Electrical Conductivity Enhancement of Transparent Silver Nanowire Films on Temperature-Sensitive Flexible Substrates Using Intense Pulsed Ion Beam. *Nanotechnology* **2021**, *32*, 145706. [CrossRef]
90. Schopp, N.; Brus, V.V.; Nguyen, T.-Q. On Optoelectronic Processes in Organic Solar Cells: From Opaque to Transparent. *Adv. Opt. Mater.* **2021**, *9*, 2001484. [CrossRef]
91. Sayigh, A. *Sustainability, Energy and Architecture: Case Studies in Realizing Green Buildings*; Academic Press: Boston, MA, USA, 2013; p. iii. ISBN 978-0-12-397269-9.
92. Kirk, A.P. Chapter 1—Energy Demand and Solar Electricity. In *Solar Photovoltaic Cells*; Kirk, A.P., Ed.; Academic Press: Oxford, UK, 2015; pp. 1–8. ISBN 978-0-12-802329-7.
93. Traverse, C.J.; Pandey, R.; Barr, M.C.; Lunt, R.R. Emergence of Highly Transparent Photovoltaics for Distributed Applications. *Nat. Energy* **2017**, *2*, 849. [CrossRef]
94. Yang, C.; Liu, D.; Bates, M.; Barr, M.C.; Lunt, R.R. How to Accurately Report Transparent Solar Cells. *Joule* **2019**, *3*, 1803–1809. [CrossRef]
95. Schubert, E.F. *Light-Emitting Diodes*, 2nd ed.; E. Fred Schubert: Troy, NY, USA, 2006; ISBN 978-0-9863826-1-1.
96. Xue, Q.; Xia, R.; Brabec, C.J.; Yip, H.-L. Recent Advances in Semi-Transparent Polymer and Perovskite Solar Cells for Power Generating Window Applications. *Energy Environ. Sci.* **2018**, *11*, 1688–1709. [CrossRef]
97. Lunt, R.R.; Bulovic, V. Transparent, near-Infrared Organic Photovoltaic Solar Cells for Window and Energy-Scavenging Applications. *Appl. Phys. Lett.* **2011**, *98*, 113305. [CrossRef]
98. Chang, S.-Y.; Cheng, P.; Li, G.; Yang, Y. Transparent Polymer Photovoltaics for Solar Energy Harvesting and Beyond. *Joule* **2018**, *2*, 1039–1054. [CrossRef]
99. Lunt, R.R. Theoretical Limits for Visibly Transparent Photovoltaics. *Appl. Phys. Lett.* **2012**, *101*, 043902. [CrossRef]
100. Tuchinda, C.; Srivannaboon, S.; Lim, H.W. Photoprotection by Window Glass, Automobile Glass, and Sunglasses. *J. Am. Acad. Dermatol.* **2006**, *54*, 845–854. [CrossRef]
101. Preto, S.; Gomes, C.C. Lighting in the Workplace: Recommended Illuminance (Lux) at Workplace Environs. In Proceedings of the International Conference on Applied Human Factors and Ergonomics, Washington, DC, USA, 24–28 July 2019; Springer International Publishing: Cham, Switzerland, 2019; pp. 180–191.
102. Hu, Z.; Wang, J.; Ma, X.; Gao, J.; Xu, C.; Yang, K.; Wang, Z.; Zhang, J.; Zhang, F. A Critical Review on Semitransparent Organic Solar Cells. *Nano Energy* **2020**, *78*, 105376. [CrossRef]
103. Yan, C.; Barlow, S.; Wang, Z.; Yan, H.; Jen, A.K.-Y.; Marder, S.R.; Zhan, X. Non-Fullerene Acceptors for Organic Solar Cells. *Nat. Rev. Mater.* **2018**, *3*, 18003. [CrossRef]

104. Wadsworth, A.; Moser, M.; Marks, A.; Little, M.S.; Gasparini, N.; Brabec, C.J.; Baran, D.; McCulloch, I. Critical Review of the Molecular Design Progress in Non-Fullerene Electron Acceptors towards Commercially Viable Organic Solar Cells. *Chem. Soc. Rev.* **2019**, *48*, 1596–1625. [CrossRef]
105. Ou, Q.-D.; Li, Y.-Q.; Tang, J.-X. Light Manipulation in Organic Photovoltaics. *Adv. Sci.* **2016**, *3*, 1600123. [CrossRef]
106. Wang, D.; Qin, R.; Zhou, G.; Li, X.; Xia, R.; Li, Y.; Zhan, L.; Zhu, H.; Lu, X.; Yip, H.-L.; et al. High-Performance Semitransparent Organic Solar Cells with Excellent Infrared Reflection and See-Through Functions. *Adv. Mater.* **2020**, *32*, 2001621. [CrossRef]
107. Sheriff, H.K.M.; Li, Y.; Qu, B.; Forrest, S.R. Aperiodic Optical Coatings for Neutral-Color Semi-Transparent Organic Photovoltaics. *Appl. Phys. Lett.* **2021**, *118*, 033302. [CrossRef]
108. Xie, Y.; Xia, R.; Li, T.; Ye, L.; Zhan, X.; Yip, H.-L.; Sun, Y. Highly Transparent Organic Solar Cells with All-Near-Infrared Photoactive Materials. *Small Methods* **2019**, *3*, 1900424. [CrossRef]
109. Li, Y.; He, C.; Zuo, L.; Zhao, F.; Zhan, L.; Li, X.; Xia, R.; Yip, H.-L.; Li, C.-Z.; Liu, X.; et al. High-Performance Semi-Transparent Organic Photovoltaic Devices via Improving Absorbing Selectivity. *Adv. Energy Mater.* **2021**, *11*, 2003408. [CrossRef]
110. Li, Y.; Ji, C.; Qu, Y.; Huang, X.; Hou, S.; Li, C.-Z.; Liao, L.-S.; Guo, L.J.; Forrest, S.R. High Efficiency Semi-Transparent Organic Photovoltaics. In Proceedings of the 2019 IEEE 46th Photovoltaic Specialists Conference (PVSC), Chicago, IL, USA, 16–21 June 2019; pp. 0098–0100.
111. Yao, N.; Wang, J.; Chen, Z.; Bian, Q.; Xia, Y.; Zhang, R.; Zhang, J.; Qin, L.; Zhu, H.; Zhang, Y.; et al. Efficient Charge Transport Enables High Efficiency in Dilute Donor Organic Solar Cells. *J. Phys. Chem. Lett.* **2021**, *12*, 5039–5044. [CrossRef]
112. Schopp, N.; Akhtanova, G.; Panoy, P.; Arbuz, A.; Chae, S.; Yi, A.; Kim, H.J.; Promarak, V.; Nguyen, T.Q.; Brus, V.V. Unraveling Device Physics of Dilute-Donor Narrow Band Gap Organic Solar Cells with Highly Transparent Active Layers. *Advanced Mater.* **2022**. [CrossRef]
113. Hussain, K.; Kaiser, W.; Gagliardi, A. Effect of Polymer Morphology on Dilute Donor Organic Solar Cells. *J. Phys. Chem. C* **2020**, *124*, 3517–3528. [CrossRef]
114. Hu, Z.; Wang, J.; Wang, Z.; Gao, W.; An, Q.; Zhang, M.; Ma, X.; Wang, J.; Miao, J.; Yang, C.; et al. Semitransparent Ternary Nonfullerene Polymer Solar Cells Exhibiting 9.40% Efficiency and 24.6% Average Visible Transmittance. *Nano Energy* **2019**, *55*, 424–432. [CrossRef]
115. Xu, C.; Jin, K.; Xiao, Z.; Zhao, Z.; Ma, X.; Wang, X.; Li, J.; Xu, W.; Zhang, S.; Ding, L.; et al. Wide Bandgap Polymer with Narrow Photon Harvesting in Visible Light Range Enables Efficient Semitransparent Organic Photovoltaics. *Adv. Funct. Mater.* **2021**, *31*, 2107934. [CrossRef]
116. Albes, T.; Xu, L.; Wang, J.; Hsu, J.W.P.; Gagliardi, A. Origin of Photocurrent in Fullerene-Based Solar Cells. *J. Phys. Chem. C* **2018**, *122*, 15140–15148. [CrossRef]
117. Murthy, L.N.S.; Kramer, A.; Zhang, B.; Su, J.-M.; Chen, Y.-S.; Wong, K.-T.; Vandenberghe, W.G.; Hsu, J.W.P. Energy Levels in Dilute-Donor Organic Solar Cell Photocurrent Generation: A Thienothiophene Donor Molecule Study. *Org. Electron.* **2021**, *92*, 106137. [CrossRef]
118. Brus, V.V.; Proctor, C.M.; Ran, N.A.; Nguyen, T.-Q. Capacitance Spectroscopy for Quantifying Recombination Losses in Nonfullerene Small-Molecule Bulk Heterojunction Solar Cells. *Adv. Energy Mater.* **2016**, *6*, 1502250. [CrossRef]
119. Vollbrecht, J.; Brus, V.V.; Ko, S.-J.; Lee, J.; Karki, A.; Cao, D.X.; Cho, K.; Bazan, G.C.; Nguyen, T.-Q. Quantifying the Nongeminate Recombination Dynamics in Nonfullerene Bulk Heterojunction Organic Solar Cells. *Adv. Energy Mater.* **2019**, *9*, 1901438. [CrossRef]
120. Schopp, N.; Brus, V.V.; Lee, J.; Dixon, A.; Karki, A.; Liu, T.; Peng, Z.; Graham, K.R.; Ade, H.; Bazan, G.C.; et al. Effect of Palladium-Tetrakis(Triphenylphosphine) Catalyst Traces on Charge Recombination and Extraction in Non-Fullerene-Based Organic Solar Cells. *Adv. Funct. Mater.* **2021**, *31*, 2009363. [CrossRef]
121. Street, R.A. Electronic Structure and Properties of Organic Bulk-Heterojunction Interfaces. *Adv. Mater.* **2016**, *28*, 3814–3830. [CrossRef] [PubMed]
122. Street, R.A.; Krakaris, A.; Cowan, S.R. Recombination Through Different Types of Localized States in Organic Solar Cells. *Adv. Funct. Mater.* **2012**, *22*, 4608–4619. [CrossRef]
123. Brus, V.V. Light Dependent Open-Circuit Voltage of Organic Bulk Heterojunction Solar Cells in the Presence of Surface Recombination. *Org. Electron.* **2016**, *29*, 1–6. [CrossRef]
124. Brus, V.V.; Schopp, N.; Ko, S.-J.; Vollbrecht, J.; Lee, J.; Karki, A.; Bazan, G.C.; Nguyen, T.-Q. Temperature and Light Modulated Open-Circuit Voltage in Nonfullerene Organic Solar Cells with Different Effective Bandgaps. *Adv. Energy Mater.* **2021**, *11*, 2003091. [CrossRef]
125. Schopp, N.; Nguyen, T.-Q.; Brus, V.V. Optical Expediency of Back Electrode Materials for Organic Near-Infrared Photodiodes. *ACS Appl. Mater. Interfaces* **2021**, *13*, 27217–27226. [CrossRef]